Journal of ELECTRONIC MATERIALS, Vol. 50, No. 4, 2021
https://doi.org/10.1007/s11664-020-08262-z

ASIAN CONSORTIUM ACCMS–INTERNATIONAL CONFERENCE ICMG 2020

High-Pressure Structural and Electronic Properties of Potassium-Based Green Primary Explosives

B. MOSES ABRAHAM ,[1] N. YEDUKONDALU,[1,2] and G. VAITHEESWARAN[3,4]

1.—Advanced Centre of Research in High Energy Materials (ACRHEM), University of Hyderabad, Prof. C. R. Rao Road, Gachibowli, Hyderabad, Telangana 500046, India. 2.—Centre for Molecular Modeling, CSIR-Indian Institute of Chemical Technology, Tarnaka, Hyderabad 500007, India. 3.—School of Physics, University of Hyderabad, Prof. C. R. Rao Road, Hyderabad 500046, India. 4.—e-mail: vaithee@uohyd.ac.in

Recently synthesized green primary explosives potassium 4,4′-bis(dinitromethyl)-3,3′-azofurazanate (K_2BDAF) and potassium 1,1′-dinitramino-5,5′-bistetrazolate (K_2DNABT) offer fast, powerful initiation capacity and high-performance detonation characteristics to replace the long-standing toxic primary explosives. In the present study, we report the structural and electronic properties of the emerging green primary explosives K_2BDAF and K_2DNABT under hydrostatic pressure up to 10 GPa. We observed that dispersion correction methods are important for capturing weak intermolecular interactions in order to accurately describe the geometries of the primary explosives. The computed ground state structural properties using optB86b-vdW method are in good agreement with the experimental results. The pressure-dependent lattice constants and bond parameters show anisotropic nature and also a sharp discontinuity around 4–5 GPa. The obtained equilibrium bulk modulus shows that K_2BDAF is softer than K_2DNABT. Bonding analysis revealed that the C-NO_2 energetic functional groups are more sensitive than the stable ring structure under hydrostatic pressure. The calculated electronic structure of K_2BDAF using the Tran–Blaha-modified Becke–Johnson (TB-mBJ) potential shows a direct-to-indirect band gap transition around 5 GPa, which is consistent with the aforementioned discontinuity of the structure, while K_2DNABT is found to be a direct-band-gap insulator in the studied pressure range of 1–10 GPa. The abnormal trends in the structural and electronic properties suggest that K_2BDAF may undergo a structural transition/distortion around 4–5 GPa of pressure.

Key words: Green primary explosives, density-functional theory, high-pressure, electronic properties

INTRODUCTION

Continuing interest in the search for novel energetic materials is driven by the endless demand in both military and civilian sectors. Several efforts have been taken to predict/synthesize green primary explosives with desirable sensitivity, powerful initiation capacity and enhanced performance to meet the challenging requirements of the future. During the past half-decade, a wide range of green primary explosives have been synthesized to replace the long-standing toxic lead azide (LA) and lead styphnate (LS), which can detonate a variety of explosive devices from blasting caps to ballistic missiles. Copper(I) 5-nitrotetrazolate (DBX-1) is preferred as a best drop-in replacement for lead azide, but recent studies have shown the instability of DBX-1 by decomposition into periodate salts,

(Received March 4, 2020; accepted June 9, 2020; published online June 25, 2020)

which makes this material an inactive explosive.[1] Thermally stable tetra(ammine)di(5-nitrotetrazolate-N^2)cobalt(III) perchlorate (BNCP)[2] and penta(ammine)(5-cyanotetrazolate-N^2)cobalt(III) perchlorate (CP)-based primary explosives[3] are unacceptable due to their toxic perchlorate content. Thus, greater focus is needed on developing less toxic and thermally stable green primary explosives that might serve as substitutes for LA and LS. Potassium is an interesting element not only for sustaining life on earth[4,5] but also for defending human life by utilizing potassium in defense applications.[6] Szimhardt and co-workers[7] recently synthesized new metal complexes of 1,1′-dinitramino-5,5′-bitetrazole and found that potassium-based green primary explosives were potential candidates due to their reasonable sensitivity together with good thermal stability around 200°C. Hence, potassium can be considered as a best replacement for lead in designing lead-free (green) primary explosives. For instance, green primary explosives synthesized by replacing the heavy metal with potassium include 5,7-dinitro-[2,1,3]-benzoxadiazol-4-olate 3-oxide (KDNP),[8] dipotassium 3,4-bis(3-dinitromethylfurazan-4-oxy)furazan (K_2BDFOF),[6] potassium 1,1′-dinitramino-5,5′-bistetrazolate (K_2DNABT),[9] potassium 4,4′-bis(dinitromethyl)-3,3′-azofurazanate (K_2BDAF),[10] potassium 5,5′-azobis(1-nitraminotetrazolate) (K_2ABNAT)[11] and potassium salt of 1,5-di(nitramino)tetrazole (K_2DNAT).[12] In general, the detonation velocities for primary explosives are in the range of 3.5–5.5 km/s.[13] However, the detonation characteristics of advanced green primary explosives are in the range of secondary explosives. The calculated detonation pressure (D_p) and velocity (D_v) for recently synthesized green primary explosives are as follows: K_2BDFOF (D_p = 32.93 GPa, D_v = 8.43 km/s),[6] K_2DNABT (D_p = 31.7 GPa, D_v = 8.33 km/s),[9] K_2BDAF (D_p = 30.1 GPa, D_v = 8.138 km/s),[10] K_2ABNAT (D_p = 31.5 GPa, D_v = 8.367 km/s)[11] and K_2DNAT (D_p = 52.2 GPa, D_v = 10.01 km/s).[12] The last of these is the most effective green primary explosive known to date.[12]

Among the green primary explosives, K_2BDAF is a derivative of azofurazanate which is found to have impact sensitivity, detonation velocity and pressure comparable to the emerging green primary explosives. On the one hand, several experimental and theoretical studies have been carried out on furazan-based derivatives to construct complex molecules.[14–17] Xiaohong et al.[18] calculated the heat of formation (HOF) of four furazan rings that are connected by the linkage of azo (-N=N-) and azoxy groups (-N=N(O)-) and reported that the azo group enhanced the heat of formation for the furazan derivatives when compared with that of the azoxy group. Zhang et al.[19] performed DFT calculations to study the HOF, electronic structure, thermal stability and energetic properties of a series of bridged difurazan derivatives (-CH_2-CH_2-, -CH=CH-, -NH-NH-, -N=N-, -N(O)=N-) and found that the substituent groups (-ONO_2, -NH_2, -NF_2, -N_3, -NO_2) attached to the difurazan derivatives enhanced the detonation properties together with the thermal stability. On the other hand, high pressure is a powerful tool that can easily alter weak intermolecular interactions, thereby inducing structural phase transitions or even new polymorphs of explosive materials, which can play an important role in determining the performance of an explosive. Therefore, it is interesting to investigate the structural and electronic properties of K_2BDAF compared with K_2DNABT under high pressure.

METHOD OF COMPUTATION

All the calculations were performed using the projector-augmented wave (PAW) method, as implemented in the Vienna Ab initio Simulation Package (VASP)[20] based on density-functional theory (DFT). The effects of the exchange–correlation (XC) functional were taken into account through the generalized gradient approximation (GGA) with Perdew–Burke–Ernzerhof (PBE) parameterization.[21] The following plane-wave basis set was used for the calculations: $2s^2 2p^2$ for carbon, $2s^2 2p^3$ for nitrogen, $2s^2 2p^4$ for oxygen and $4\,s^1$ for potassium atoms, with the core electrons replaced by the PAW method.[22] By performing total energy convergence for the plane-wave basis orbitals, a plane-wave kinetic energy cutoff of 600 eV was found, and the Brillouin zone was sampled using $6 \times 4 \times 3$ for K_2BDAF and $5 \times 4 \times 3$ for K_2DNABT according to the Monkhorst–Pack grid scheme.[23] The structural relaxation was performed until the maximum force on each atom was less than 0.01 eV/Å. The standard DFT functionals fail to predict the densities of energetic materials,[24–26] partially due to their inadequacy in describing the non-covalent interactions such as hydrogen bonding and van der Waals (vdW) interactions[27–29] within the crystal structure. An accurate description of dispersion interactions is required to predict the structural properties of any molecular crystal. However, the recent development of vdW corrections has enabled greater accessibility of conventional DFT for the study of a wider class of problems, leading to considerable progress in electronic structure calculations.[30–34] To include the missing dispersion interactions, we incorporated two kinds of dispersion corrections: the pairwise-additive dispersion correction[35] and the non-local correction.[36,37] With the pairwise correction method, dispersion correction energy is added to the internuclear energy term that strengthens the total energy coming from a standard DFT calculation. The non-local van der Waals density functional (vdW-DF) uses the electronic charge density as an input and incorporates the non-local correlation contribution to the semi-local exchange functionals. It is well known that the electronic band gap obtained from standard DFT functionals such as

local-density approximation (LDA)[38] and GGA[21] are strongly underestimated due to self-interaction error and are unable to account for derivative discontinuity in the XC functional. In order to overcome this problem, we have used the semi-local Tran–Blaha-modified Becke–Johnson (TB-mBJ) potential, which can provide reliable band gaps for semiconductors and insulators.[39]

RESULTS AND DISCUSSION

Crystal Structure and Its Pressure Dependence

Potassium-based green primary explosives such as K_2BDAF and K_2DNABT crystallize in the triclinic crystal symmetry with space group P-1 and comprise one molecule (Z = 1) per unit cell. The crystal and molecular structure of K_2BDAF is shown in Fig. 1a–d. The crystal structure of K_2BDAF consists of two furazan rings, each with two C=N and two N-O bonds that can enhance the oxygen balance and density, thereby improving the detonation performance.[10] The furazan rings presented in the structure are joined by the linkage of an azo group (-N=N-), which further improves the HOF.[40,41] In addition, the dinitromethyl group attached to the furazan rings adds extra flavor in the efficient construction of high-energy-density material.[42,43] The K_2DNABT structure consists of nitramino groups attached to the tetrazole units that contain a greater number of N-N bonds, which can boost the performance, with better thermal stability, due to the aromaticity related to the ring.[44] When compared with K_2BDAF, the presence of more nitrogen bonding networks in K_2DNABT leads to higher detonation properties with reasonable stability. In order to determine the appropriate method for describing the structural properties, we optimized the structural lattice parameters of both compounds using different functionals, which are presented in Table I along with the experimental values.[9,10] The obtained results without including the dispersion correction method show a larger deviation from the experimental values, especially the overestimation of the volume by around 12.2% (10.2%) for K_2BDAF (K_2DNABT) using the standard PBE-GGA functional. This discrepancy is improved by using dispersion correction. For instance, the calculated volume of K_2BDAF using the DFT-D2 method is overestimated by 2.9%, whereas with the non-local dispersion-corrected method it is underestimated by around 0.3% and 0.7% using the optB86b-vdW and optB88-vdW methods, respectively. Overall, the optB86b-vdW

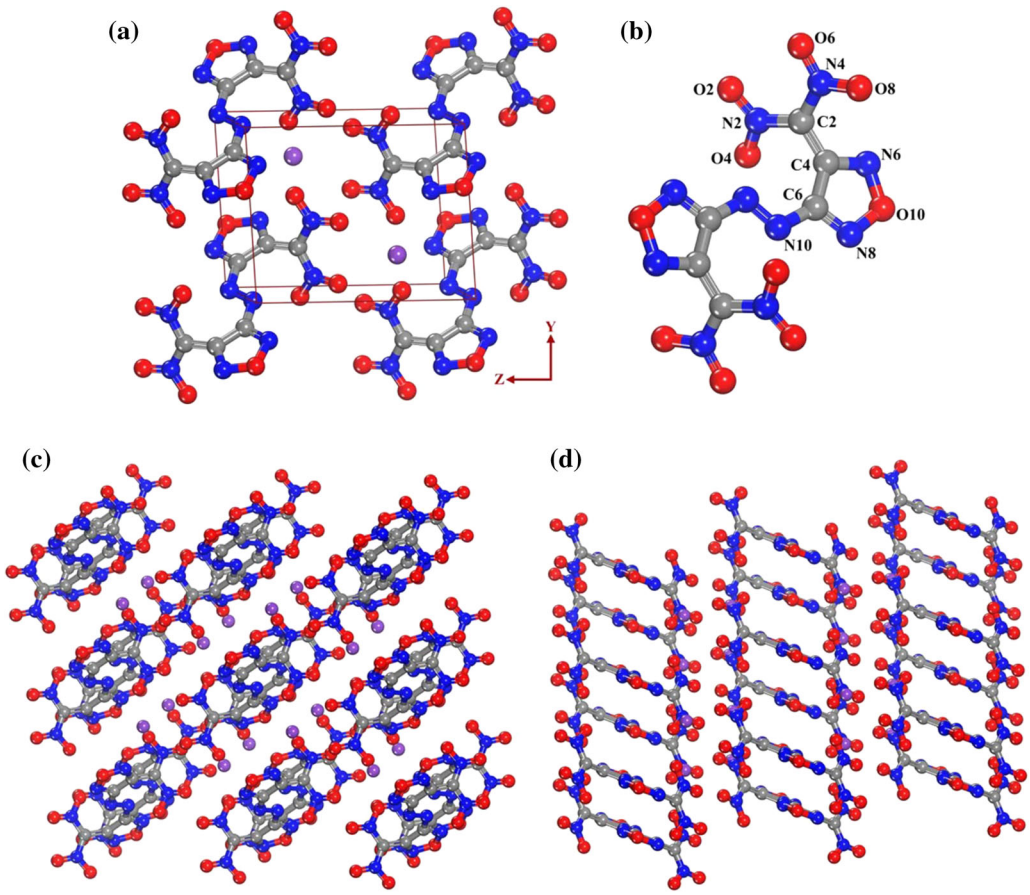

Fig. 1. (a) Triclinic (P-1) unit cell, (b) single molecular geometry of 4,4′-bis(dinitromethyl)-3,3′-azofurazanate anion, (c) and (d) layer assembly mode of K_2BDAF structure.

Table I. Calculated lattice constants (a, b, c, α, β, γ) and volume (V) of K_2BDAF and K_2DNABT using PBE-GGA and dispersion-corrected functionals along with experimental values

	Method	PBE	D2	optB86b	optB88	Expt[9,10]
K_2BDAF	a (Å)	5.256 (+6.6%)	5.982 (21.4%)	4.910 (−0.4%)	4.908 (−0.4%)	4.929
	b (Å)	7.678 (+2.1%)	7.602 (+1.1%)	7.561 (+0.6%)	7.558 (+0.6%)	7.517
	c (Å)	10.122 (+3.5%)	9.851 (+0.7%)	9.706 (−0.8%)	9.663 (−1.2%)	9.780
	α (°)	81.33 (−2.1%)	82.82 (−0.3%)	83.51 (+0.5%)	83.86 (+1.0%)	83.07
	β (°)	83.46 (−0.8%)	84.35 (+0.3%)	84.28 (+0.2%)	84.61 (+0.6%)	84.11
	γ (°)	86.35 (+0.1%)	85.44 (−0.2%)	86.01 (+0.4%)	86.12 (+0.5%)	85.65
	V (Å^3)	400.8 (+12.2%)	367.6 (+2.9%)	356.2 (−0.3%)	354.7 (−0.7%)	357.1
K_2DNABT	a (Å)	5.183 (+1.7%)	5.136 (+0.8%)	5.090 (−0.1%)	5.086 (−0.2%)	5.096
	b (Å)	7.043 (+3.1%)	6.830 (+0.1%)	6.756 (−1.0%)	6.761 (−0.9%)	6.824
	c (Å)	8.482 (+3.2%)	8.450 (+0.3%)	8.431 (+0.1%)	8.436 (+0.1%)	8.427
	α (°)	68.93 (+2.0%)	67.17 (−0.6%)	67.41 (−0.2%)	67.17 (−0.5%)	67.56
	β (°)	87.15 (+1.2%)	86.12 (−0.1%)	86.39 (+0.3%)	86.39 (+0.3%)	86.15
	γ (°)	72.36 (+1.9%)	71.13 (+0.2%)	71.19 (+0.2%)	71.11 (+0.1%)	71.02
	V (Å^3)	281.7 (+10.2%)	258.0 (+0.9%)	252.7 (−1.1%)	252.4 (−1.3%)	255.6

The relative errors (in %) when compared with experiments are shown in parentheses. The plus (+) and minus (−) signs represent the over- and underestimation of the calculated values with respect to the experimental results[9,10]

method is in good accord with the experimental results under ambient conditions and confirms that the intermolecular interactions are accurately described by this method for the studied compounds.

In our previous study,[45] we explored the structure and spectroscopic properties of K_2DNABT under high pressure. K_2DNABT shows structural distortion in the pressure range of 5–6 GPa, which motivated us to carry out high-pressure study of the isostructural compound K_2BDAF. The compression behavior of lattice constants is depicted in Fig. 2a. It is observed that the lattice parameters of K_2BDAF change unevenly in the pressure range of 4–5 GPa, suggesting that the K_2BDAF crystal structure may undergo structural distortion/transition similar to K_2DNABT. For instance, in the range of 4–5 GPa, the trends for lattice constants a, b and c are quite different: a decreases, b increases, and c is invariant. When the pressure is increased from 5 GPa to 10 GPa, a and c decrease, while b gradually increases, revealing the anisotropic compressibility of K_2BDAF under high pressure. Similar behavior is observed even in the pressure–volume curve, with a sudden discontinuity at 4 GPa, as shown in Fig. 2c. On the other hand, the unit cell volume exhibits a large compression ratio near the low-pressure region. For instance, the volume is reduced by 13.6% in the region of 0–5 GPa, which is much greater than that (7.7%) in the pressure region of 5–10 GPa. In the low-pressure region, the molecules are far apart from each other, and thus the crystal is easily compressed due to the weak intermolecular interactions in the crystal. As pressure increases, the intermolecular repulsion also increases, and it becomes difficult to further compress the crystal. The calculated normalized cell parameters and volume as a function of pressure are shown in Fig. 2b and d. The variations in the normalized cell parameters have large differences, suggesting the anisotropic nature of K_2BDAF under compression. It is found that the lattice constant a decreases rapidly below 4 GPa, with an abrupt change around 4–5 GPa indicating a possible structural transition, and then slowly decreases up to 10 GPa, while the b and c lattice constants increase abruptly at 5 GPa. However, in the pressure range of 5–10 GPa, the order of compressibility along different directions is $a > c > b$, indicating that the crystal structure of K_2BDAF is much stiffer in the crystallographic b direction than in the a and c directions. The abrupt changes in all these lattice constants imply that the structure of K_2BDAF may undergo a marked transition around 4–5 GPa. Further, the change in unit cell volume as a function of pressure for K_2BDAF is fitted to a third-order Birch–Murnaghan equation of state, and the computed bulk modulus (B_0) and its pressure derivatives (B'_0) are found to be 16.2 GPa and 6.38, respectively. The smaller value of B_0 (16.2 GPa) obtained for the studied compound indicates the softer nature of the compound when compared with K_2DNABT (22.4 GPa),[45] while the metal organic framework $Zn(GlyTyr)_2$ reported by Sanchez et al.[46] shows a bulk modulus of 21.9 GPa, which indicates that the material is harder than K_2BDAF and softer than K_2DNABT. Further, these B_0 values reveal that the studied primary explosives K_2DNABT and K_2BDAF are softer than inorganic primary explosives $Pb(N_3)_2$ (26 GPa[47] and 41 GPa[48]) and AgN_3 (39 GPa, 27.6 GPa),[49,50] and

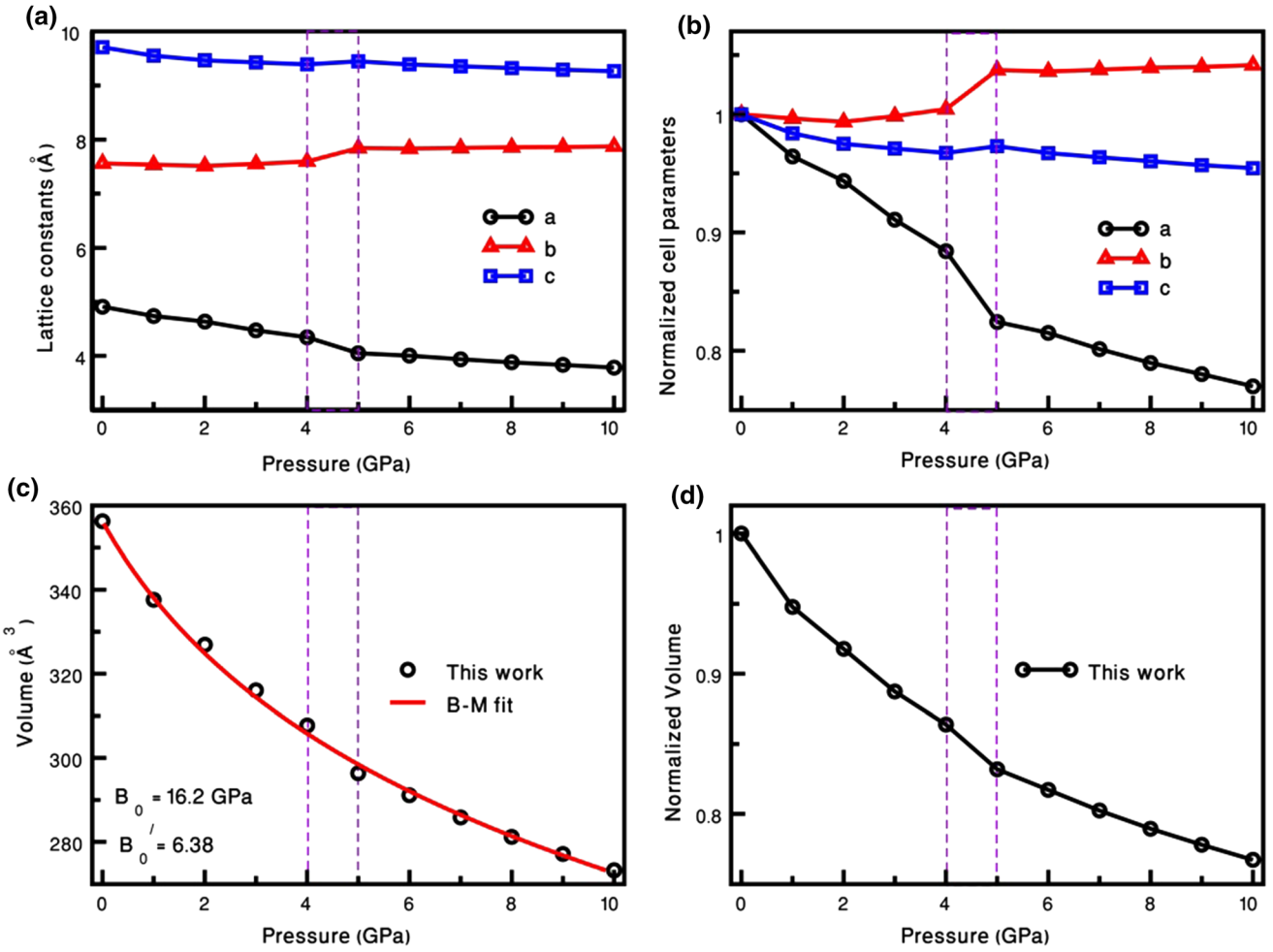

Fig. 2. Calculated (a) lattice parameters (a, b, c), (b) normalized lattice parameters (a/a_0, b/b_0, c/c_0), (c) volume (V) and (d) normalized volume (V/V_0) of K_2BDAF under the studied pressure range.

harder than the very sensitive[51] organic primary explosive C_3N_{12} (12.6 GPa).[52]

Inter- and Intramolecular Interactions

Inter- and intramolecular interactions play a crucial role in the stability of molecular crystals. These non-covalent interactions can be easily tuned by high pressure, thereby inducing the polymorphism or structural phase transitions which further lead to the formation of novel phases. Therefore, it is interesting to study the behavior of molecular crystals under hydrostatic compression. The variations in the unit cell of K_2BDAF under pressure are mainly due to changes in the bond lengths and angles of the molecular geometry of the anion. The bond lengths of the C-NO_2 group and ring structure of K_2BDAF with increasing pressure are plotted in Fig. 3a and b. In particular, we are interested in the C-NO_2 group, which is more sensitive to bending and rotation than the stable ring structure under compression. The C2-N2 and N4-O8 bond lengths decrease rapidly as a function of pressure, indicating that the C2-N2 and N4-O8 bonds weaken more easily than other bonds under compression. Therefore, the C-NO_2 group may undergo severe deformation leading to rupture with increasing pressure. In addition, the N2-O2, N2-O4, N4-O8, C2-N2 and C2-N4 bond lengths show an abrupt change in the pressure range of 4–5 GPa. The bond lengths of the ring structure show only a slight change and remain unchanged under compression. Pressure-dependent lattice angles also show a discontinuity between 4 GPa and 5 GPa of pressure (see Fig. 3c and d), indicating a possible structural distortion/transition in K_2BDAF in the pressure range of 4–5 GPa.

Electronic Structure Under High Pressure

Most energetic materials are semiconductors or insulators; therefore, the electronic structure (especially band gap) plays a crucial role in their photodecomposition mechanisms. Unfortunately, the standard DFT functionals cannot precisely reproduce the electronic band gap trends when compared with the experiments. As discussed in section II, TB-mBJ potential provides reasonably good band gaps for semiconductors and insulators

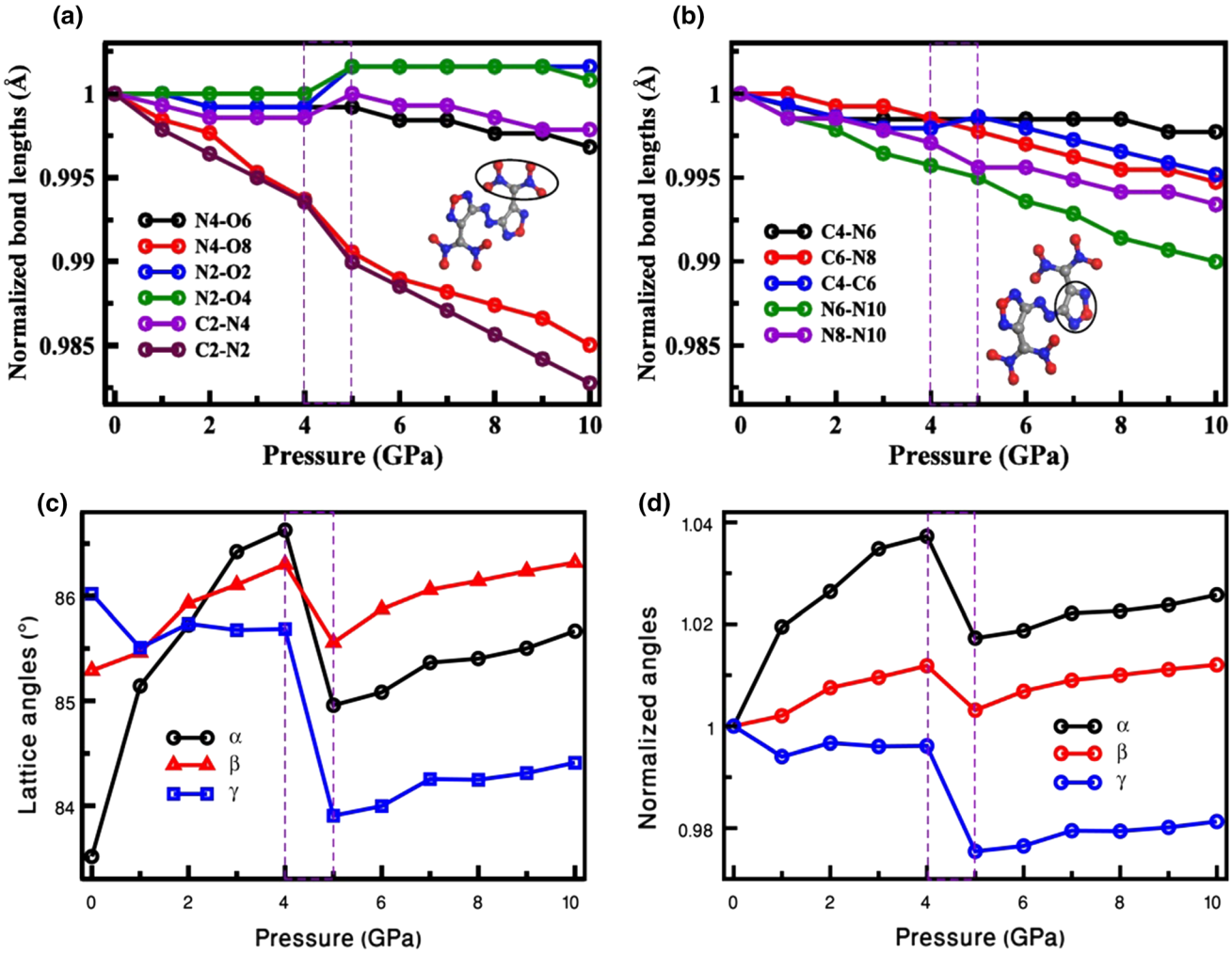

Fig. 3. Calculated (a) and (b) normalized bond lengths, (c) lattice angles (α, β, γ), (d) normalized lattice angles (α/α_0, β/β_0, γ/γ_0) of K_2BDAF as a function of pressure.

compared with more sophisticated hybrid functionals and GW approximation. Therefore, the electronic structure of K_2DNABT and K_2BDAF is computed using TB-mBJ potential at both ambient and high pressure. As it is well known that the effect of pressure can alter the electronic properties of these emerging green primary explosives, the pressure dependence of the band gap using TB-mBJ potential was investigated up to 10 GPa in steps of 1 GPa. The calculated band structures of both compounds along the high symmetry directions of the Brillouin zone using TB-mBJ potential are presented in Fig. 4a–f. At ambient pressure, K_2BDAF is found to have a direct band gap of 2.081 eV along the B-B direction. By comparing the electronic band structure at ambient and high pressure, we found that the pressure had a marked effect on the electronic band gap nature of the material. When the pressure reached 5 GPa, the conduction band minimum (CBM) shifted from the B- to the F-direction, while the valance band maximum (VBM) remained in the B-direction. As a result, K_2BDAF transitioned from a direct to an indirect band gap material and it retained the indirect band gap nature up to the maximum pressure of the present study, i.e., 10 GPa. Peng et al.[53] also studied the electronic properties of the secondary explosive β-HMX under hydrostatic pressure using first principles calculations and reported a transition in the electronic band structure from a direct to an indirect band gap at elevated pressures. They also reported that the decrease in band gap as a function of pressure is due to the variation in electronic charge density. On the other hand, K_2DNABT is found to be a direct-band-gap insulator along the B-direction over the studied pressure range. The band gap values at various pressures are reported in Table II. The results of our previous studies on K_2DNABT[45] and K_2BDAF[54] using the full-potential linearized augmented plane wave method performed using WIEN2K are in excellent agreement with the electronic band gap obtained using the PAW method. The band gap as a function of pressure for K_2DNABT and K_2BDAF compounds is

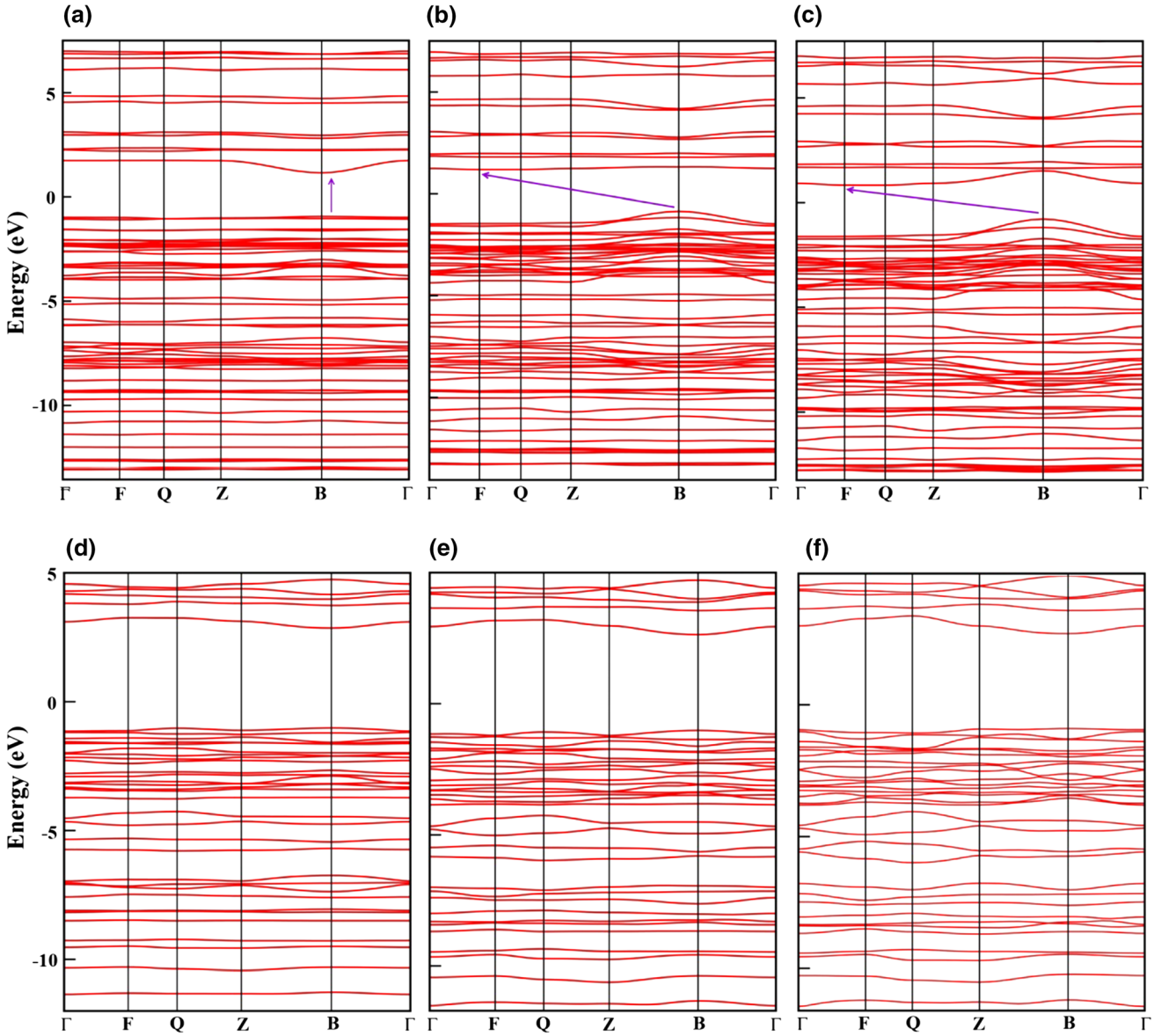

Fig. 4. Calculated electronic band structure of K_2BDAF and K_2DNABT using TB-mBJ potential at 0 GPa (a, d), 5 GPa (b, e) and 10 GPa (c, f), respectively.

Table II. The calculated band gaps (eV) of K_2BDAF and K_2DNABT using GGA and TB-mBJ potential.

	Pressure (GPa)	PBE-GGA	TB-mBJ	Direction
K_2BDAF	0	1.46	2.08	B–B
	5	1.46	2.04	B–F
	10	1.07	1.61	B–F
K_2DNABT	0	3.01	3.87	B–B
	5	2.90	3.65	B–B
	10	2.96	3.59	B–B

shown in Fig. 5a and b. As the pressure increases, the band gap of K_2BDAF decreases, with a discontinuity around 5 GPa. This abnormal trend around 4–5 GPa is consistent with the variation tendency of lattice parameters, which is provoked by the structural distortion around 5 GPa in the case of K_2BDAF. It is observed that the reduction in band gap in the high-pressure region is more pronounced

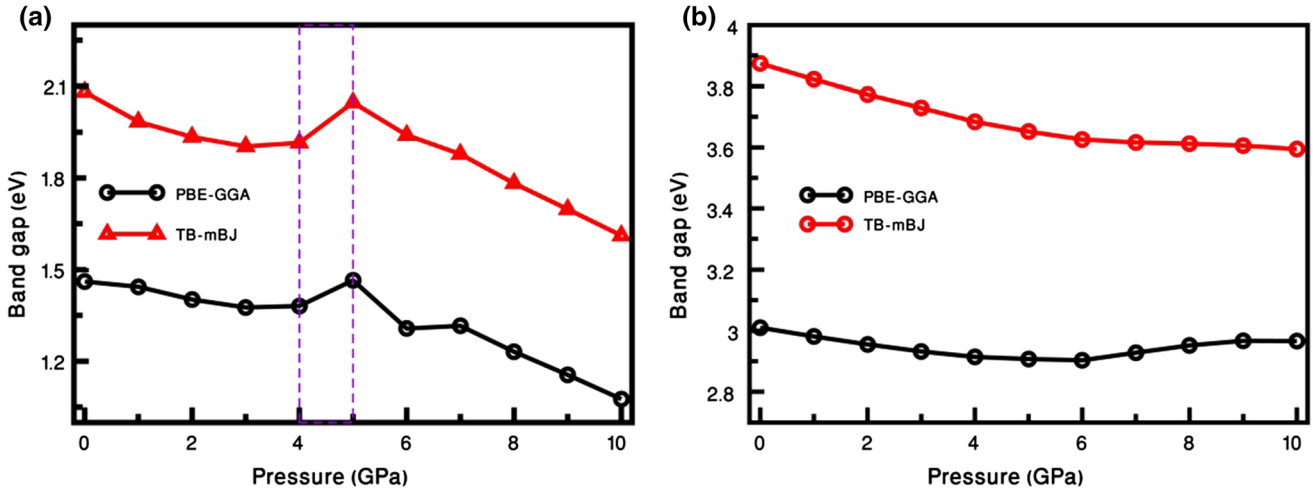

Fig. 5. Calculated band gap values as a function of pressure up to 10 GPa for (a) K_2BDAF and (b) K_2DNABT using TB-mBJ potential.

than in the low-pressure region, while the band gap decreases with increasing pressure for K_2DNABT. Younk et al.[55] also reported band gap lowering in lead azide due to the reduction of intermolecular spacing under compression. Overall, K_2DNABT has a higher band gap than K_2BDAF, which shows that K_2DNABT is less photo-sensitive than K_2BDAF.

In order to gain a better understanding of the electronic structure of the green primary explosives, we investigated the total density of states (DOS) and partial DOS (PDOS) of K_2BDAF and K_2DNABT under pressure of 0 GPa and 10 GPa, as shown in Fig. 6a and b. For K_2BDAF, the VBM is due mainly to C-states that are attached to the nitro group and O states of the NO_2 group. It can be expected that the contribution of the latter to the valence band is greater than that of the former. This indicates that the C atom attached to the nitro group behaves like an active center. With increasing pressure, the electrons from the C states attached to the NO_2 group become denser and more dispersive. Therefore, there is a possibility of C-NO_2 bond fusion under compression. On the other hand, the CBM is dominated by p states of the N4 and N5 atoms, with much less contribution from the p states of the O5 atoms. Further, the 2*p* states of N1, N2, O1, O2, O3 and O4 atoms are found to occur in the same energy range of −5 eV to −10 eV and show strong hybridization, reflecting the covalent nature of the NO_2 group. Similar behavior was observed even in the case of K_2DNABT, where the N1, O1 and O2 atoms show strong bonding in the same energy range. Meanwhile, the VBM of K_2DNABT is due mainly to the N5 atoms attached to the nitro group and the oxygen (O1 and O2) atoms of the NO_2 group.

As the pressure increases, the bands of K_2BDAF show greater dispersion, tending to shift towards a lower-energy region. Generally, such peculiarities in the broadening of the DOS, showing an increase in the band splitting and dispersion, are mainly due to an increase in the intermolecular interactions under compression.[56] Further, the gap between the VB and CB decreases, indicating the probability of electronic excitation under pressure.[57] We can also expect a semiconducting nature in K_2BDAF under high pressure, which shows that K_2BDAF is more sensitive and becomes easier to decompose and explode under pressure. This is supported by the results of various experimental studies, where the sensitivity of explosives to detonation initiation increases with applied pressure. By comparison, the bands of K_2DNABT show little difference under pressure. This indicates that the sensitivity of K_2DNABT remains unchanged in the studied pressure range.

CONCLUSIONS

In summary, we conducted a comparative study of the structural and electronic properties of K_2BDAF and K_2DNABT under pressure of up to 10 GPa using first principles calculations with the inclusion of dispersion correction methods to capture the weak intermolecular interactions. The obtained structural properties are very well reproduced (with deviation of 0.3%) using optB86b-vdW when compared with the experimental results. The effect of pressure on the lattice constants and bond parameters reveals the anisotropic nature and sharp discontinuities around 4–5 GPa for K_2BDAF. The computed bulk moduli indicate that K_2BDAF is a softer material than K_2DNABT. The calculated electronic properties using TB-mBJ potential at ambient conditions show that K_2BDAF has a direct band gap (2.08 eV) along the B-direction, which transforms to an indirect band gap (2.05 eV to 1.61 eV) along the B–F direction under pressure from 5 GPa to 10 GPa. Meanwhile, K_2DNABT is found to be a direct-band-gap insulator in the calculated pressure range. The band gap of K_2BDAF gradually decreases, with a discontinuity observed at 5 GPa, while the band gap first decreases and then

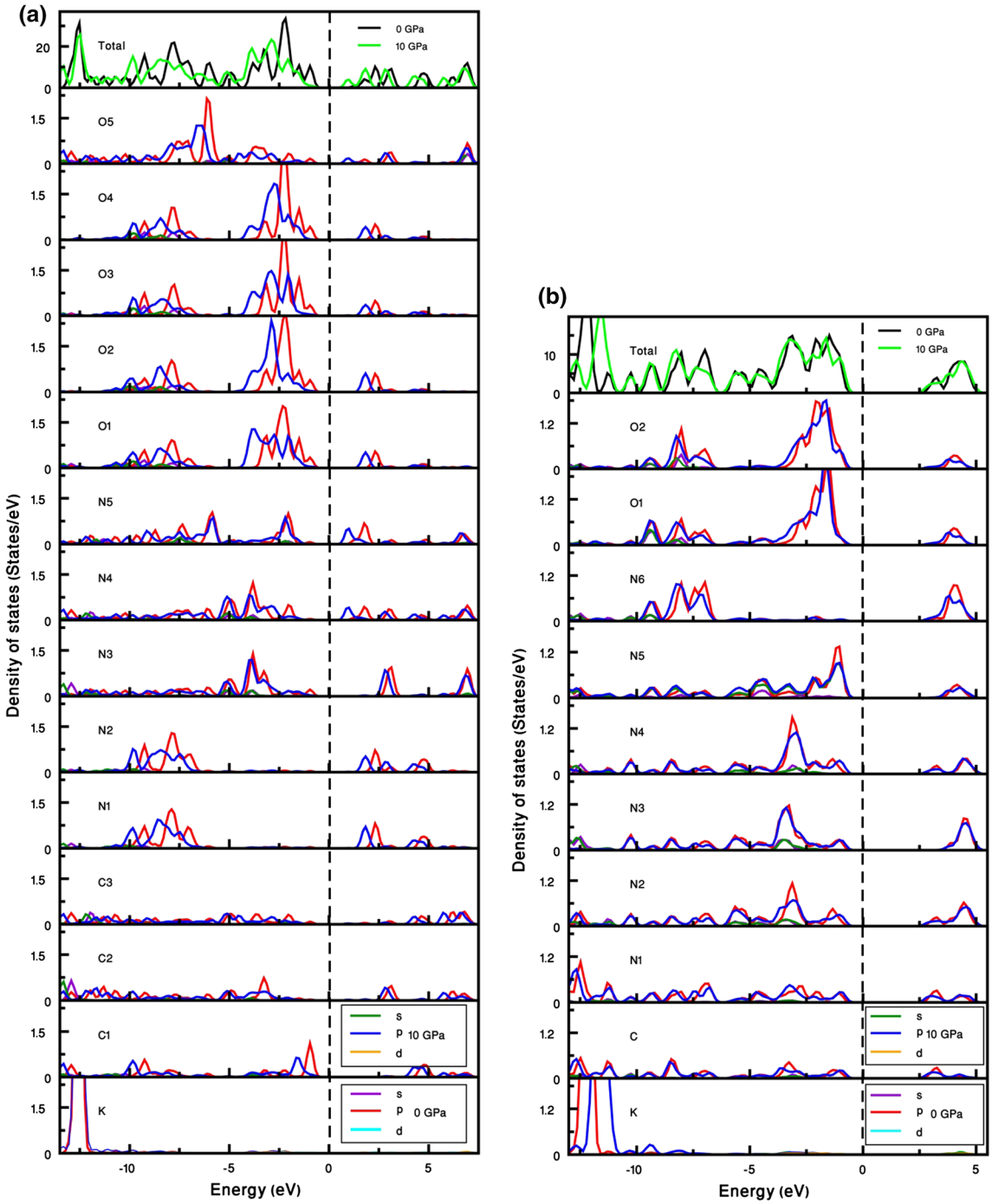

Fig. 6. Calculated partial density of states of (a) K_2BDAF, (b) K_2DNABT at 0 GPa and 10 GPa using TB-mBJ potential.

increases slightly with pressure for K_2DNABT. Overall, the structural and electronic properties of the investigated primary explosives as a function of pressure suggest that the K_2BDAF and K_2DNABT may undergo a structural phase distortion/transition around 4–5 GPa. The crystal structure of K_2BDAF and K_2DNABT under high pressure is an open challenge and will be solved using crystal structure prediction methods in the near future.

ACKNOWLEDGMENTS

BMA would like to thank the Defence Research and Development Organization (DRDO), Ministry of Defence, Govt. of India, for financial support under Grant No. DRDO/18/1801/2016/01038:ACREHM-PHASEIII, and the Centre for Modelling Simulation & Design (CMSD), University of Hyderabad, for providing computational facilities.

CONFLICT OF INTEREST

The authors declare that they have no conflict of interest.

REFERENCES

1. T.M. Klapötke, D.G. Piercey, N. Mehta, K.D. Oyler, and J.J. Sabatini, *Z. Naturforsch.* 69b, 125 (2014).
2. A.J. Grimley, J.G. Harlan, and J.W. Fronabarger, *Proceedings of the 16th International Pyrotechnics Seminar*, p. 785 (1991).
3. W.B. Leslie, R.W. Dietzel, and J.Q. Searcy, *Proceedings of the 6th Symposium (International) on Detonation*, p. 455 (1976).
4. L.Y. Chen, J.G. Zhang, Z.N. Zhou, and T.L. Zhang, *RSC Adv.* 6, 98381 (2016).
5. F. Kukita, *J. Membr. Biol.* 242, 119 (2011).
6. L. Zhai, X. Fan, B. Wang, F. Bi, Y. Li, and Y. Zhu, *RSC Adv.* 5, 57833 (2015).
7. N. Szimhardt, M.F. Bölter, M. Born, T.M. Klapötke, and J. Stierstorfer, *Dalton Trans.* 46, 5033 (2017).
8. J.W. Fonabarger, M.D. Williams, W.B. Sanborn, D.A. Parrish, and M. Bichay, *Prop. Explos. Pyrotech.* 36, 459 (2011).
9. D. Fischer, T.M. Klapötke, and J. Stierstorfer, *Angew. Chem. Int. Ed.* 53, 8172 (2014).
10. Y. Tang, C. He, L.A. Mitchell, D.A. Parrish, and J.M. Shreeve, *Angew. Chem. Int. Ed.* 55, 5565 (2016).
11. Y.N. Li, B.Z. Wang, Y.J. Shu, L.J. Zhai, S.Y. Zhang, F.Q. Bi, and Y.C. Li, *Chin. Chem. Lett.* 28, 117 (2017).
12. D. Fischer, T.M. Klapötke, and J. Stierstorfer, *Angew. Chem. Int. Ed.* 54, 10299 (2015).
13. K. Akhavan, *Royal Society of Chemistry* (*Cambridge,* 2004).
14. Y. Tang, J. Zhang, L.A. Mitchell, D.A. Parrish, and J.M. Shreeve, *J. Am. Chem. Soc.* 137, 15984 (2015).
15. J. Zhang, S. Dharavath, L.A. Mitchell, D.A. Parrish, and J.M. Shreeve, *J. Mater. Chem. A* 4, 16961 (2016).
16. M.B. Talawar, R. Sivabalan, N. Senthilkumar, G. Prabhu, and S.N. Asthana, *J. Hazard. Mater.* A113, 11 (2004).
17. M. Xia, Y. Chu, T. Wang, W. Lei, and F. Wang, *J. Mol. Model.* 22, 268 (2016).
18. L. Xiaohong, Z. Ruizhou, and Z. Xianzhou, *Struct. Chem.* 24, 1193 (2013).
19. X. Zhang, W. Zhu, and H. Xiao, *J. Phys. Chem. A* 114, 603 (2010).
20. G. Kresse and J. Furthmuller, *Phys. Rev. B* 54, 11169 (1996).
21. J.P. Perdew, K. Burke, and M. Ernzerhof, *Phys. Rev. Lett.* 77, 3865 (1997).
22. P.E. Blöchl, *Phys. Rev. B* 50, 17953 (1994).
23. H.J. Monkhorst and J.D. Pack, *Phys. Rev. B* 13, 5188 (1976).
24. E.F.C. Byrd and B.M. Rice, *J. Phys. Chem. C* 111, 2787 (2007).
25. J. Klimes and A. Michaelides, *J. Chem. Phys.* 137, 120901 (2012).
26. E.F.C. Byrd, G.E. Scuseria, and C.F. Chabalowski, *J. Phys. Chem. B* 108, 13100 (2004).
27. M. Dion, H. Rydberg, E. Schroder, D.C. Langreth, and B.I. Lundqvist, *Phys. Rev. Lett.* 92, 246401 (2004).
28. B. Santra, J. Klimes, D. Alfe, A. Tkatchenko, B. Slater, A. Michaelides, R. Car, and M. Scheffler, *Phys. Rev. Lett.* 107, 185701 (2011).
29. D. Lu, Y. Li, D. Rocca, and G. Galli, *Phys. Rev. Lett.* 102, 206411 (2009).
30. S. Hunter, P. Coster, A. Davidson, D. Millar, S. Parker, W. Marshall, R. Smith, C. Morrison, and C. Pulham, *J. Phys. Chem. C* 119, 2322 (2015).
31. C. Cazorla, D. Errandonea, and E. Sola, *Phys. Rev. B* 80, 064105 (2009).
32. A.C. Landerville, M.W. Conroy, M.M. Budzevich, Y. Lin, C.T. White, and I.I. Oleynik, *Appl. Phys. Lett.* 97, 251908 (2010).
33. D.C. Sorescu and B.M. Rice, *J. Phys. Chem. C* 114, 6734 (2010).
34. A.K. Sagotra, D. Errandonea, and C. Cazorla, *Nat. Commun.* 8, 963 (2017).
35. S. Grimme, *J. Comput. Chem.* 27, 1787 (2006).
36. J. Klimes, D.R. Bowler, and A. Michaelides, *Phys. Rev. B* 83, 195131 (2011).
37. J. Klimes, D.R. Bowler, and A. Michaelides, *J. Phys. Condens. Matter* 22, 022201 (2010).
38. D.M. Ceperley and B.J. Alder, *Phys. Rev. Lett.* 45, 566 (1980).
39. F. Tran and P. Blaha, *Phys. Rev. Lett.* 102, 226401 (2009).
40. A.A. Dippold, T.M. Klapötke, and Z. Anorg, *Allg. Chem.* 637, 1453 (2011).
41. P. Yin, D.A. Parrish, and J.M. Shreeve, *Chem. Eur. J.* 20, 6707 (2014).
42. C. He and J.M. Shreeve, *Angew. Chem. Int. Ed.* 55, 772 (2016).
43. X. Zhao, S. Li, Y. Wang, Y. Li, F. Zhao, and S. Pang, *J. Mater. Chem. A* 4, 5495 (2016).
44. D. Chand, D.A. Parrish, and J.M. Shreeve, *J. Mater. Chem. A* 1, 15383 (2013).
45. N. Yedukondalu and G. Vaitheeswaran, *J. Chem. Phys.* 143, 064508 (2015).
46. J.N. Sanchez, I.M. Ruíz, C. Popescu, D.S. Perez, A. Segura, D. Errandonea, J.G. Platas, and C.M. Gastaldo, *Dalton Trans.* 10654, 47 (2018).
47. D.I.A. Millar, *Energetic Materials at Extreme Conditions* (Berlin: Springer, 2012).
48. C.E. Weir, S. Block, and G.J. Piermarini, *J. Chem. Phys.* 53, 4265 (1970).
49. D. Hou, F. Zhang, C. Ji, T. Hannon, H. Zhu, J. Wu, V.I. Levitas, and Y. Ma, *J. Appl. Phys.* 110, 023524 (2011).
50. N. Yedukondalu G. Vaitheeswaran, P. Modak, L. Ashok, and K. Verma, *Solid State Comm.* 297, 39 (2019).
51. J.P. Agrawal and R. Hodgson, *Organic Chemistry of Explosives* (New York: Wiley, 2007).
52. S. Appalakondaiah, G. Vaitheeswaran, and S. Lebégue, *Chem. Phys. Lett.* 605, 10 (2014).
53. Q. Peng, G. Rahul, G.R. Wang, S.De Liu, and S. Pang, *Phys. Chem. Chem. Phys.* 16, 1997 (2014).
54. E.N. Rao and G. Vaitheeswaran, *J. Phys. Chem. C* 123, 10034 (2019).
55. E.H. Younk and A.B. Kunz, *Int. J. Quantum Chem.* 63, 615 (1997).
56. W. Qiong, Z. Weihua, and X. Heming, *Struct. Chem.* 25, 451 (2014).
57. L. Zhichao, W. Qiong, Z. Weihua, and X. Heming, *Can. J. Chem.* 92, 616 (2014).